

Stellar dynamics in razor-thin discs with massive nuclear black holes

Mir Abbas Jalali[★]

Institute for Advanced Studies in Basic Sciences, PO Box 45195-159, Gava Zang, Zanjan, Iran

Accepted 1999 June 28. Received 1999 June 8; in original form 1999 March 3

ABSTRACT

The bifurcations of orbit-averaged dynamics are studied in a class of razor-thin discs with central black holes. The model used here consists of a perturbed harmonic oscillator Hamiltonian augmented with a $-GM/r$ potential. Through a sequence of conformal and canonical transformations, we reduce the phase-space flows of the system to a set of non-linear differential equations on a sphere. Based on the critical points of the averaged system, we classify orbit families and reveal the existence of six types of periodic motions: *circular*, *long- and short-axis elliptical*, *long- and short-axis radial* and *inclined radial* orbits. Long-axis elliptical orbits and their surrounding *tubes* have significant features: whilst they keep stars away from the centre, they elongate in the same direction as the density profile. These properties are helpful in the construction of self-consistent equilibria.

Key words: celestial mechanics, stellar dynamics – galaxies: kinematics and dynamics.

1 INTRODUCTION

It is widely believed that most galactic nuclei might be powered by massive objects. Central black holes (BHs) are the best candidates for supporting this hypothesis. Nuclear BHs may contain 2.5 per cent of the mass of their host galaxies (Merritt & Quinlan 1998, hereafter MQ; Kormendy & Richstone 1995). Although a BH creates relativistic effects, it can be modelled as a Newtonian point mass at distances greater than Schwarzschild’s radius. This simplifies the theoretical framework of dynamical studies. In a pioneering work, Goodman & Binney (1984) showed that a gradual accumulation of mass at the central regions of stellar systems forces the tangential components of velocity dispersion to grow more than the radial components. This is an evidence of evolution toward a steady symmetric state, which has been confirmed by the N -body simulations of MQ. In this way, Merritt & Valluri (1996) revealed the importance of chaotic mixing. The approach from triaxiality to axisymmetry is through the destruction of the *box* orbits that are needed to maintain non-axisymmetric shapes. In the presence of central BHs, Sridhar & Touma (1997, 1999, hereafter ST) reported that the box orbits of non-axisymmetric stellar discs are replaced by a new family of orbits, the *lenses*. The geometry of the lens orbits can elucidate the stability of cuspy, non-axisymmetric discs.

In this paper we show that the combined gravitational fields of the nuclear BH and the host galaxy stabilize two families of regular orbits, *long- and short-axis elliptical tubes*, which coexist with the lens orbits. The long-axis tubes can support the highly non-axisymmetric shapes of stellar discs. At first we introduce a class of elliptical galaxies with quadratic density distributions and

locate a point mass at the galaxy centre. By squeezing the short axis of our triaxial system to zero length, we obtain a non-axisymmetric, razor-thin disc and extract its orbital content. Our model is a quartic extension of the centred ST discs. The nuclear BH contributes a singularity to the Hamiltonian function. We remove the singularity by utilizing the Levi–Civita transformation and then express the Hamiltonian in the Lissajous variables. By performing a ‘second-order’ Lie transformation and transferring to Hopf’s coordinates, we end up with a normalized Hamiltonian system on a two-dimensional sphere. We classify the possible families of orbits using the equilibrium points of the reduced system. Finally, we discuss two examples of non-axisymmetric discs and investigate the bifurcations of orbits when the ratio $M_{\text{g}}/M_{\text{g}}$ (BH mass to galaxy mass) takes various values.

2 HAMILTONIAN FUNCTION

In the past decades, several models have been developed to describe the distribution of matter inside elliptical galaxies. For galaxies with finite core densities, the following model has provided satisfactory results (Jalali & Sobouti 1998):

$$\rho = \text{sgn}(1 - m^2)\rho_0(1 - m^2)^n, \quad (1)$$

$$m^2 = \frac{x^2}{a^2} + \frac{y^2}{b^2} + \frac{z^2}{c^2}, \quad a \geq b \geq c,$$

where a , b and c are the semi-axes of the ellipsoid describing the galaxy surface. The constant ρ_0 denotes the core density and n is an integer number that controls the steepness of ρ . In this paper we consider $n = 1$, which results in a total mass of $M_{\text{g}} = 8\pi\rho_0 abc/15$ for the galaxy. The gravitational potential associated with the assumed ρ is determined through the relation

[★]E-mail: jalali@iasbs.ac.ir

(Chandrasekhar 1969)

$$U = \frac{-\pi}{2} G \rho_0 abc \int_0^\infty \left(1 - \frac{x^2}{a^2 + u} - \frac{y^2}{b^2 + u} - \frac{z^2}{c^2 + u} \right)^2 \frac{du}{\Delta(u)}, \quad (2)$$

with $\Delta(u) = [(a^2 + u)(b^2 + u)(c^2 + u)]^{1/2}$. After expanding the integrand, one achieves

$$U = U_0 \left(-\frac{1}{4} a_{00} + \frac{a_{11}}{2a^2} x^2 + \frac{a_{22}}{2a^2} y^2 + \frac{a_{33}}{2a^2} z^2 - \frac{b_{11}}{4a^4} x^4 - \frac{b_{22}}{4a^4} y^4 - \frac{b_{33}}{4a^4} z^4 - \frac{a_{12}}{2a^4} x^2 y^2 - \frac{a_{13}}{2a^4} x^2 z^2 - \frac{a_{23}}{2a^4} y^2 z^2 \right), \quad (3)$$

where $U_0 = 2\pi G \rho_0 bc$. The constant coefficients a_{ij} and b_{ii} are presented in Appendix A as functions of $e_1 = b/a$ and $e_2 = c/a$. We place a point mass (black hole) at the centre of the galaxy by adding a potential of the form $-GM_b/\sqrt{x^2 + y^2 + z^2}$ to U , with M_b being the mass of the central body. Thus, the Hamiltonian function can be written as follows:

$$\mathcal{H} = \frac{1}{2}(p_x^2 + p_y^2 + p_z^2) + U(x, y, z) - \frac{GM_b}{\sqrt{x^2 + y^2 + z^2}}, \quad (4)$$

where p_x, p_y and p_z are the momenta conjugate to x, y and z , respectively. We now compress the short axis to zero length, i.e. $e_2 \rightarrow 0$. This gives us a non-axisymmetric, razor-thin disc. Therefore, motions will be confined to the x - y plane and the dynamics is governed by the following dimensionless Hamiltonian:

$$\bar{\mathcal{H}} = \frac{\mathcal{H}}{U_0} + \frac{1}{4} a_{00} = \frac{1}{2}(\bar{p}_x^2 + \bar{p}_y^2) + \Phi(\bar{x}, \bar{y}) - \frac{\mu}{\sqrt{\bar{x}^2 + \bar{y}^2}}, \quad (5)$$

$$\Phi = \frac{1}{2} \omega^2 \bar{x}^2 + \frac{1}{2} \lambda^2 \bar{y}^2 - \frac{1}{4} \alpha \bar{x}^4 - \frac{1}{4} \gamma \bar{y}^4 - \frac{1}{2} \beta \bar{x}^2 \bar{y}^2,$$

$$\mu = \frac{4 M_b}{15 M_g},$$

where

$$\bar{x} = \frac{x}{a}, \quad \bar{y} = \frac{y}{a}, \quad \bar{t} = \frac{\sqrt{U_0}}{a} t, \quad (6)$$

and $(\omega^2, \lambda^2, \beta, \alpha, \gamma) = \lim_{e_2 \rightarrow 0} (a_{11}, a_{22}, a_{12}, b_{11}, b_{22})$. From and (6), one finds the allowable region of internal motions:

$$\bar{x}^2 + \frac{\bar{y}^2}{e_1^2} \leq 1. \quad (7)$$

3 REGULARIZATION

Let us apply the Levi-Civita transformation

$$\begin{aligned} \bar{x} &= u^2 - v^2, \\ \bar{y} &= 2uv. \end{aligned} \quad (8)$$

In fact, u and v are parabolic coordinates. According to (8), one obtains the regularized Hamiltonian

$$\mathcal{K} = \frac{1}{2}(p_u^2 + p_v^2) + J(\Phi(u, v) - h), \quad (9)$$

$$J = 4(u^2 + v^2), \quad p_u = \frac{du}{d\tau},$$

$$p_v = \frac{dv}{d\tau}, \quad d\bar{t} = J d\tau,$$

where τ is the new independent variable, J is the Jacobian of the conformal transformation (8), (p_u, p_v) is the momentum vector associated with (u, v) and $h \equiv \bar{\mathcal{H}} = \text{constant}$. Any motion generated by \mathcal{K} takes place on the manifold $\mathcal{K} = 4\mu$ (see Boccaletti & Pucacco 1996 for detailed analysis). The Hamiltonian \mathcal{K} can be rewritten as

$$\mathcal{K} = \frac{1}{2}(p_u^2 + p_v^2) - 4h(u^2 + v^2) + \epsilon \mathcal{K}_1(u, v) + \frac{1}{2!} \epsilon^2 \mathcal{K}_2(u, v), \quad (10)$$

$$\mathcal{K}_1 = 2\omega^2(u^6 - u^4 v^2 - u^2 v^4 + v^6) + 8\lambda^2 u^2 v^2 (u^2 + v^2),$$

$$\mathcal{K}_2 = 2(u^2 + v^2)[- \alpha(u^2 - v^2)^4 - 16\gamma u^4 v^4 - 8\beta u^2 v^2 (u^2 - v^2)^2].$$

For $(u^2 + v^2) \ll 1$, we may consider \mathcal{K}_1 and \mathcal{K}_2 as the first- and second-order perturbations for the quadratic terms, respectively. The parameter ϵ is introduced to distinguish the perturbing terms from the others and will eventually be set equal to unity. In this study we consider $h < 0$, which corresponds to bounded motions when $\epsilon \rightarrow 0$.

4 NORMALIZATION

Consider the Lissajous transformation of Deprit (1991), $(u, v, p_u, p_v) \rightarrow (\ell, g, L, G)$:

$$u = s \cos(g + \ell) - d \cos(g - \ell),$$

$$v = s \sin(g + \ell) - d \sin(g - \ell),$$

$$p_u = -\Omega[s \sin(g + \ell) + d \sin(g - \ell)],$$

$$p_v = \Omega[s \cos(g + \ell) + d \cos(g - \ell)], \quad (11)$$

where

$$\Omega s^2 = \frac{1}{2}(L + G), \quad \Omega d^2 = \frac{1}{2}(L - G),$$

$$\Omega^2 = -8h(h < 0), \quad L > 0, \quad |G| \leq L.$$

Substituting from (11) into (10) yields

$$\mathcal{K} = \mathcal{K}_0 + \epsilon \mathcal{K}_1(\ell, g, L, G) + \frac{1}{2!} \epsilon^2 \mathcal{K}_2(\ell, g, L, G), \quad (12)$$

$$\mathcal{K}_0 = \Omega L.$$

From (12), one concludes that ℓ is the fast angle and g is the slow one. The variable ℓ can be eliminated from \mathcal{K} by implementing a Lie transformation $(\ell, g, L, G) \rightarrow (\ell', g', L', G')$ (Deprit 1969). Up to order 2 in ϵ , the normalized Hamiltonian is

$$\mathcal{K}' = \mathcal{K}'_0 + \epsilon \mathcal{K}'_1(g', L', G') + \frac{1}{2!} \epsilon^2 \mathcal{K}'_2(g', L', G'), \quad (13)$$

where

$$\mathcal{K}'_0 = \Omega L',$$

$$\mathcal{K}'_1 = \frac{1}{2\pi} \int_0^{2\pi} \mathcal{K}_1(\ell', g', L', G') d\ell',$$

$$\mathcal{K}'_2 = \frac{1}{2\pi} \int_0^{2\pi} [\mathcal{K}_2 + 2(\mathcal{K}_1; W_1) + ((\mathcal{K}_0; W_1); W_1)] d\ell',$$

$$\frac{\partial W_1}{\partial \ell'} = \frac{1}{\Omega} [\mathcal{K}_1(\ell', g', L', G') - \mathcal{K}'_1(g', L', G')].$$

$(f_1; f_2)$ denotes the Poisson bracket of f_1 and f_2 over the (ℓ', g', L', G') space. The primed and unprimed variables are

related by the mapping (Deprit 1969)

$$\begin{aligned}\mathcal{X} &= \mathcal{X}' + \epsilon \frac{\partial W_1}{\partial \mathcal{Y}'} + \frac{1}{2!} \epsilon^2 \left[\frac{\partial W_2}{\partial \mathcal{Y}'} + \left(\frac{\partial W_1}{\partial \mathcal{Y}'}; W_1 \right) \right], \\ \mathcal{Y} &= \mathcal{Y}' - \epsilon \frac{\partial W_1}{\partial \mathcal{X}'} - \frac{1}{2!} \epsilon^2 \left[\frac{\partial W_2}{\partial \mathcal{X}'} + \left(\frac{\partial W_1}{\partial \mathcal{X}'}; W_1 \right) \right],\end{aligned}\quad (14)$$

where $\mathcal{X} \equiv (\ell, g)$, $\mathcal{Y} \equiv (L, G)$ and

$$\frac{\partial W_2}{\partial \mathcal{L}'} = \frac{1}{\Omega} [\mathcal{K}_2 + 2(\mathcal{K}_1; W_1) + ((\mathcal{K}_0; W_1); W_1) - \mathcal{K}'_2]. \quad (15)$$

The normalization procedure has been performed by a symbolic mathematical processor. The result is

$$\begin{aligned}\mathcal{K}'_1 &= c_0 + c_1 s'^2 d'^2 + c_2 s'^2 d'^2 \cos 4g', \\ \mathcal{K}'_2 &= c_3 + c_4 s'^2 d'^2 + c_5 s'^4 d'^4 + c_6 s'^4 d'^4 \cos 8g' \\ &\quad + c_7 s'^2 d'^2 \cos 4g' + c_8 s'^4 d'^4 \cos 4g',\end{aligned}\quad (16)$$

where $c_i s$ are constants and can be determined through the relations given in Appendix B. It is seen that ℓ' has become cyclic, leaving its conjugate momentum L' as a constant of the motion. L' is the *second integral* in our planar problem (h is the first integral of motion). Following the prospects of Deprit & Eliepe (1991), we carry out a transformation to Hopf's coordinates (Q_1, Q_2, Q_3) :

$$\begin{aligned}Q_1 &= \frac{1}{2\Omega} \sqrt{L'^2 - G'^2} \cos 2g', \\ Q_2 &= \frac{1}{2\Omega} \sqrt{L'^2 - G'^2} \sin 2g', \\ Q_3 &= \frac{1}{2\Omega} G', \quad Q_1^2 + Q_2^2 + Q_3^2 = \frac{1}{4} \xi^2,\end{aligned}\quad (17)$$

and express the Hamiltonian in the form

$$\mathcal{K}' = C_0 + A_{20} Q_1^2 + A_{10} Q_2^2 + \frac{1}{2} A_{21} Q_1^4 + \frac{1}{2} A_{12} Q_2^4 + C Q_1^2 Q_2^2, \quad (18)$$

with $\xi = L'/\Omega$. The constant coefficients $C_0, C, A_{20}, A_{10}, A_{12}$ and A_{21} have been defined in Appendix B. The equations of the 'averaged motion' are derived from (18):

$$\frac{dQ_i}{d\tau} = (Q_i; \mathcal{K}') \equiv \frac{\partial Q_i}{\partial g'} \frac{\partial \mathcal{K}'}{\partial G'} - \frac{\partial Q_i}{\partial G'} \frac{\partial \mathcal{K}'}{\partial g'}, \quad i = 1, 2, 3. \quad (19)$$

By employing the chain rule of differential calculus in (19) and collecting the partial derivatives of \mathcal{K}' with respect to Q_i , one can show

$$\begin{aligned}\frac{dQ_1}{d\tau} &= (Q_1; Q_2) \frac{\partial \mathcal{K}'}{\partial Q_2}, \\ \frac{dQ_2}{d\tau} &= -(Q_1; Q_2) \frac{\partial \mathcal{K}'}{\partial Q_1}, \\ \frac{dQ_3}{d\tau} &= (Q_3; Q_1) \frac{\partial \mathcal{K}'}{\partial Q_1} - (Q_2; Q_3) \frac{\partial \mathcal{K}'}{\partial Q_2}.\end{aligned}\quad (20)$$

From (17) it can be verified that

$$(Q_1; Q_2) = Q_3, \quad (Q_2; Q_3) = Q_1, \quad (Q_3; Q_1) = Q_2. \quad (21)$$

Substitution from (21) into (20) yields

$$\frac{dQ_i}{d\tau} = 2(-1)^{(i+1)} Q_j Q_k f_i, \quad i = 1, 2, 3; \quad j, k \neq i, \quad (22)$$

where

$$f_i = A_{i0} + A_{i1} Q_1^2 + A_{i2} Q_2^2 \quad (23)$$

and

$$\begin{aligned}A_{11} &= A_{22} = C, \\ A_{30} &= A_{20} - A_{10}, \quad A_{31} = A_{21} - C, \\ A_{32} &= C - A_{12}.\end{aligned}$$

The phase-space flows of (22) lie on the sphere $S^2 = \{(Q_1, Q_2, Q_3) \in \mathfrak{R}^3 | Q_1^2 + Q_2^2 + Q_3^2 = \frac{1}{4} \xi^2\}$. It is not easy to trace three-dimensional flows on S^2 . In order to visualize such flows, one can project the sphere S^2 in \mathfrak{R}^3 on to the $Q_{p1}-Q_{p2}$ plane in \mathfrak{R}^2 through the following relations:

$$Q_{p1} = \frac{Q_1}{\frac{1}{2}\xi - Q_3}, \quad Q_{p2} = \frac{Q_2}{\frac{1}{2}\xi - Q_3} \quad (24)$$

Thus, flows on the upper and lower hemispheres of S^2 ($Q_3 > 0$ and $Q_3 < 0$) are mapped on to the regions $C^+ = \{(Q_{p1}, Q_{p2}) \in \mathfrak{R}^2 | Q_{p1}^2 + Q_{p2}^2 > 1\}$ and $C^- = \{(Q_{p1}, Q_{p2}) \in \mathfrak{R}^2 | Q_{p1}^2 + Q_{p2}^2 < 1\}$, respectively. The point $(0, 0, -\frac{1}{2}\xi)$ in \mathfrak{R}^3 is projected on to the origin. The circles $Q_1^2 + Q_2^2 = \frac{1}{4}\xi^2$ (C_1), $Q_1^2 + Q_3^2 = \frac{1}{4}\xi^2$ (C_2) and $Q_2^2 + Q_3^2 = \frac{1}{4}\xi^2$ (C_3) are projected on to the unit circle $S^1 = \{(Q_{p1}, Q_{p2}) \in \mathfrak{R}^2 | Q_{p1}^2 + Q_{p2}^2 = 1\}$, the Q_{p1} -axis and Q_{p2} -axis, respectively. As equations (22) are invariant under the reflections $Q_3 \rightarrow -Q_3$ and $\tau \rightarrow -\tau$, it is sufficient to analyse the region $\mathcal{D} = C^- \cup S^1$.

5 EQUILIBRIA AND THE FAMILIES OF ORBITS

In the usual manner, the possible families of orbits can be classified using the equilibrium points (EPs) of the normalized system (22). Such points appear as periodic orbits in real space. Relying on the values of e_1, ξ and Ω , different configurations of EPs are obtained. The numerical computations of f_i show that they do not vanish simultaneously. This means that all EPs lie on the circles C_1, C_2 and C_3 . Such EPs are classified as follows.

(i) As the starting point, we consider the case in which none of f_i vanishes on C_1, C_2 and C_3 . Equivalently, we suppose that $f_i \neq 0$ for $Q_i = 0$. For $Q_3 = 0$ and $f_3 \neq 0$, we obtain $[(A_{30} + \frac{1}{4}A_{31}\xi^2)/(A_{31} - A_{32})] < 0$ on S^1 . For $Q_i = 0$ and $f_i \neq 0$ ($i = 1, 2$), we find $A_{i0}A_{ij} > 0$ ($j = 1, 2; j \neq i$). Thus, we obtain the trivial EPs

$$E_0 \equiv (0, 0), \quad E_{1,2} \equiv (\pm 1, 0), \quad E_{3,4} \equiv (0, \pm 1). \quad (25)$$

These points are the intersections of S^2 with the coordinate axes Q_1, Q_2 and Q_3 . It is remarked that the coordinates of the EPs have been given in the $Q_{p1}-Q_{p2}$ plane. E_0 corresponds to a circular orbit of radius ξ defined by $\bar{x}^2 + \bar{y}^2 = \xi^2$ (Fig. 1a). To show this we use (24) and (17). At the point E_0 , we have $Q_1 = Q_2 = 0$ and $Q_3 = -\xi/2$. Hence, from (17), we conclude that $L' = G'$, which leads to $d' = 0$ and $s'^2 = \xi$. By applying these results in (11), one achieves

$$\begin{aligned}u &= \sqrt{\xi} \cos(g + \ell), \\ v &= \sqrt{\xi} \sin(g + \ell).\end{aligned}\quad (26)$$

Substitution from (26) into (8) yields the required equation of the circular orbit. A similar scheme can be followed for extracting the physical meaning of other EPs. It is found that $E_{1,2}$ and $E_{3,4}$ denote

oscillating *radial* motions along the \bar{x} and \bar{y} axes, respectively (Fig. 1b). Such motions are periodic with a maximum amplitude of 2ξ and undergo elastic collisions at the galactic nucleus. In fact, any star approaching the nuclear black hole will be tidally shredded. Therefore, the radial motions can only exist in theory.

(ii) Non-trivial EPs on the circle C_1 (S^1 in the Q_{p1} - Q_{p2} plane) are obtained by setting $Q_3 = 0$ and $f_3 = 0$. Such points exist if $[(A_{30} + \frac{1}{4}A_{31}\xi^2)/(A_{31} - A_{32})] > 0$ on S^1 . Four EPs will be generated on S^1 :

$$E_{5,6,7,8} \equiv \frac{2}{\xi}(\pm\Delta_1, \pm\Delta_2), \quad (27)$$

$$\Delta_1 = \sqrt{\frac{A_{30} + \frac{1}{4}A_{32}\xi^2}{A_{32} - A_{31}}}, \quad \Delta_2 = \sqrt{\frac{A_{30} + \frac{1}{4}A_{31}\xi^2}{A_{31} - A_{32}}}.$$

They stand for *inclined radial* motions, as shown in Fig. 1c. The maximum amplitude δ and inclination i of these orbits are given by

$$\delta = \sqrt{\bar{x}_{\max}^2 + \bar{y}_{\max}^2} = 2\xi, \quad i = \arctan\left(\frac{\pm\Delta_2}{\pm\Delta_1}\right). \quad (28)$$

(iii) Non-trivial EPs on C_2 (the Q_{p1} -axis) are obtained when $f_2 = 0$ and $Q_2 = Q_{p2} = 0$. For $Q_2 = 0$, the equation $f_2 = 0$ has real roots if $A_{20}A_{21} < 0$ and $(\xi^2 + 4A_{20}/A_{21}) > 0$. Consequently, two EPs occur on the Q_{p1} -axis. The coordinates of these points are

$$S_{1,2} \equiv \left(\frac{\pm\sqrt{-A_{20}/A_{21}}}{\frac{1}{2}\xi + \sqrt{\frac{1}{4}\xi^2 + \frac{A_{20}}{A_{21}}}}, 0 \right). \quad (29)$$

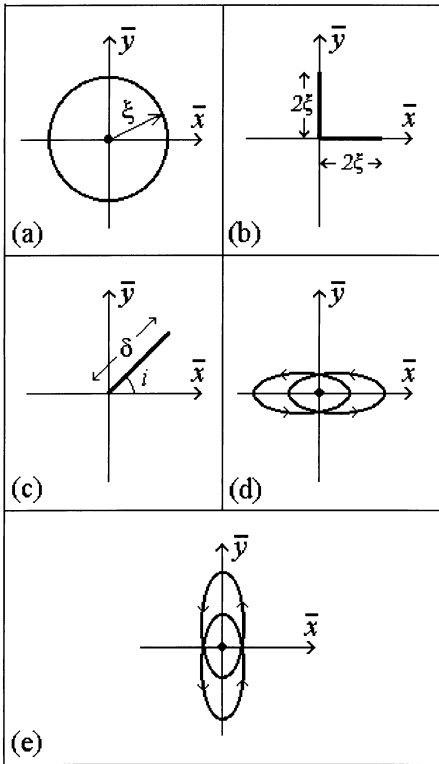


Figure 1. Periodic orbits: (a) circular orbit; (b) on-axis radial orbits; (c) inclined radial orbit; (d) long-axis elliptical orbits; (e) short-axis elliptical orbits.

They correspond to the ellipses

$$\frac{(\bar{x} \pm \bar{x}_0)^2}{a_1^2} + \frac{\bar{y}^2}{b_1^2} = 1, \quad (30)$$

$$a_1^2 = \xi^2, \quad b_1^2 = \xi^2 + 4\frac{A_{20}}{A_{21}}, \quad \bar{x}_0 = 2\sqrt{\frac{-A_{20}}{A_{21}}}.$$

Such ellipses are elongated in the \bar{x} -direction (Fig. 1d).

(iv) Non-trivial EPs on C_3 (the Q_{p2} -axis) are obtained when $f_1 = 0$ and $Q_1 = Q_{p1} = 0$. For $Q_1 = 0$, the equation $f_1 = 0$ has real roots if $A_{10}A_{12} < 0$ and $(\xi^2 + 4A_{10}/A_{12}) > 0$. Consequently, two EPs emerge on the Q_{p2} -axis. The coordinates of these points are

$$S_{3,4} \equiv \left(0, \pm \frac{\sqrt{-A_{10}/A_{12}}}{\frac{1}{2}\xi + \sqrt{\frac{1}{4}\xi^2 + \frac{A_{10}}{A_{12}}}} \right). \quad (31)$$

They are associated with elliptical orbits elongated in the \bar{y} -direction (Fig. 1e). Such ellipses are represented by

$$\frac{\bar{x}^2}{a_2^2} + \frac{(\bar{y} \pm \bar{y}_0)^2}{b_2^2} = 1, \quad (32)$$

$$b_2^2 = \xi^2, \quad a_2^2 = \xi^2 + 4\frac{A_{10}}{A_{12}}, \quad \bar{y}_0 = 2\sqrt{\frac{-A_{10}}{A_{12}}}.$$

The normalized system has no other possibilities for EPs. In our model galaxies, stellar orbits are not permitted to cross the galactic boundary. This requirement limits the value of ξ . By taking into account (7) and the amplitude of the short-axis radial motions, we find $\xi_{\max} = e_1/2$.

6 EXAMPLES

To this end, we construct the phase-space flows of equation (22) for $\xi = 0.9\xi_{\max}$ and several choices of e_1 and M_b/M_g . The results obtained have been illustrated in Fig. 2 for $e_1 = 0.5$ and in Figs 3(a)–(f) for $e_1 = 0.2$. The EPs are shown with solid dots and the circle S^1 has been drawn in each figure. The predicted periodic motions are stable if their associated stationary points are centres. Otherwise, one achieves unstable periodic motions (for the saddle-type EPs). The closed curves encircling E_0 , $S_{1,2}$ and $S_{3,4}$ produce tube orbits which are formed around the periodic motions. Thus,

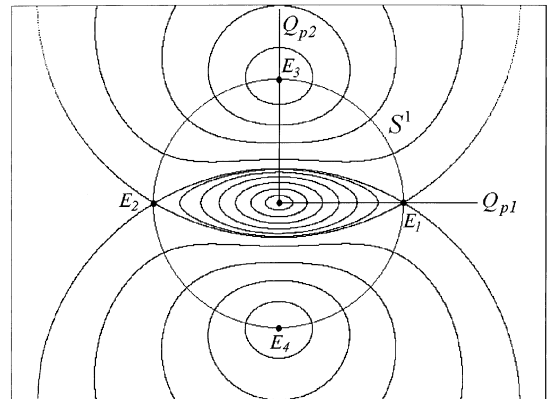


Figure 2. The projected phase-space flows of the normalized system for $e_1 = 0.5$ and $M_b/M_g = 0.02$.

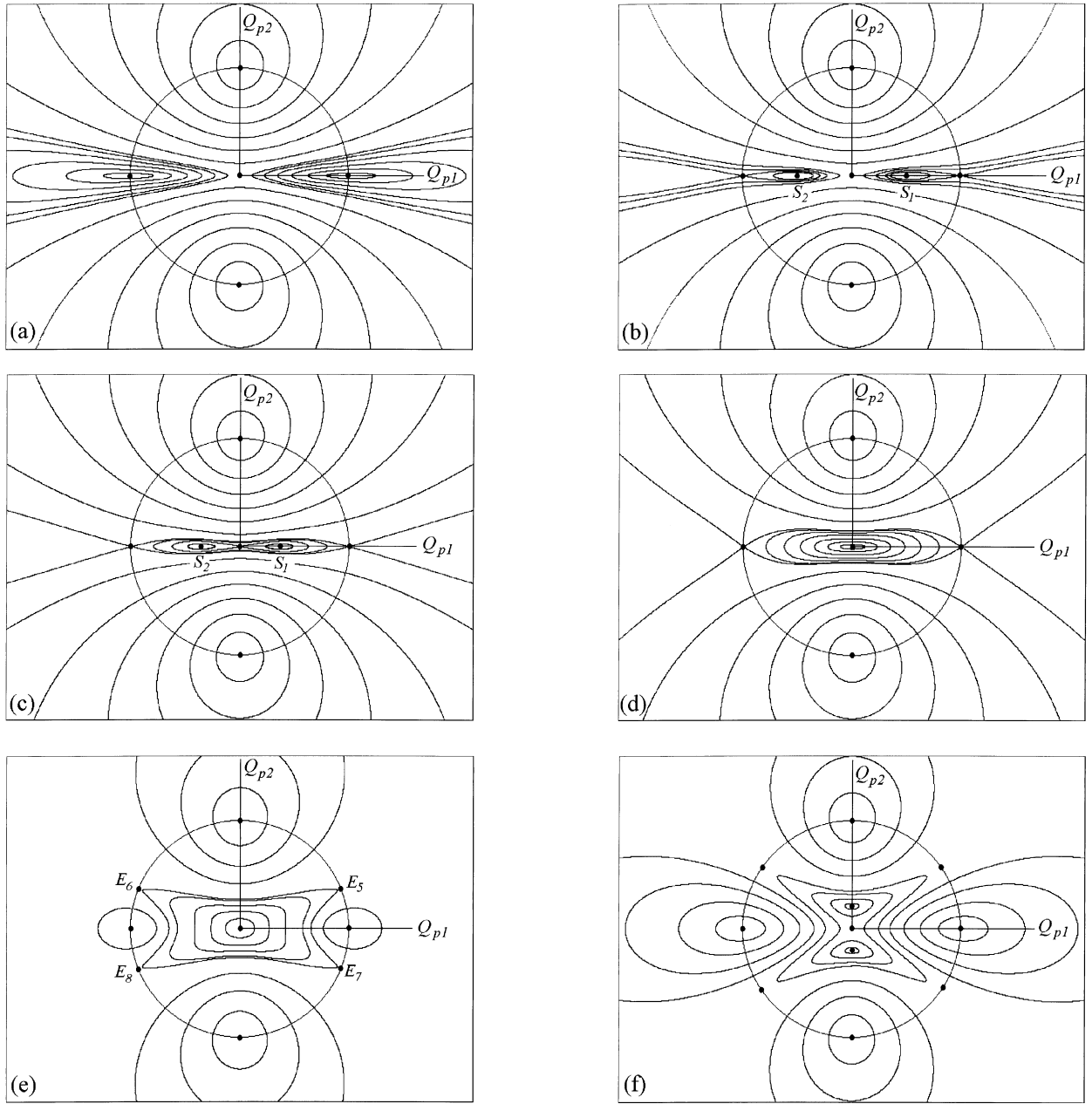


Figure 3. The projected phase-space flows of the normalized system for $e_1 = 0.2$. Solid dots indicate equilibrium points and the circle S^1 can be seen in each figure. (a) $M_b/M_g = 0.01$; (b) $M_b/M_g = 0.02$; (c) $M_b/M_g = 0.025$; (d) $M_b/M_g = 0.04$; (e) $M_b/M_g = 0.06$; (f) $M_b/M_g = 0.08$.

according to the classification made above, we acquire *circular* and *elliptical tubes* (Figs 4a and b). The closed curves crossing the circle S^1 give birth to motions for which the angular momentum G switches sign. This is the character of the *box* (de Zeeuw & Merritt 1983) and *lens* orbits. In our case we have lenses. The lenses proceed from the radial motions (EPs on the circle S^1) and therefore we obtain *short-* and *long-axis* lenses (Figs 4c and d). Ω^2 , which occurs in (18) (see also Appendix B), is approximately equal to $4\mu/\xi$. Hence, for a specified ξ , the value of Ω^2 may be controlled by the variation of the mass fraction $M_b/M_g = 15\mu/4$.

As it is evident from Fig. 2, for $e_1 = 0.5$ and $M_b/M_g = 0.02$, the short-axis lenses and circular tubes (*loops*) are the only existing families of orbits. They are generic for centred quadratic potentials when a first-order averaging is performed (see ST). Such a topology is not altered by other choices of M_b/M_g . We now

choose $e_1 = 0.2$. For $M_b/M_g = 0.01$ the long- and short-axis lenses fill all of phase space (Fig. 3a). By increasing M_b/M_g to 0.02 the long axis lenses disappear while the circular orbits are still unstable. Stable *long-axis elliptical* orbits and their surrounding tubes come into existence through the occurrence of $S_{1,2}$ (Fig. 3b). The elliptical tubes are confined to a homoclinic orbit, which connects E_1 (E_2) to itself. By further increase in M_b/M_g , S_1 and S_2 approach E_0 . Then, E_0 changes its role and become a homoclinic point (Fig. 3c). Once S_1 and S_2 reach the origin (Fig. 3d), the circular orbits become stable and a topology similar to Fig. 2 is obtained. For $M_b/M_g = 0.06$, the inclined radial motions appear as $E_{5,6,7,8}$ (Fig. 3e) and the long-axis lenses occur again. For $M_b/M_g = 0.08$ the circular motions become unstable and the *short-axis elliptical* orbits are generated, along with their surrounding tubes (Fig. 3f). We no longer continue our analysis

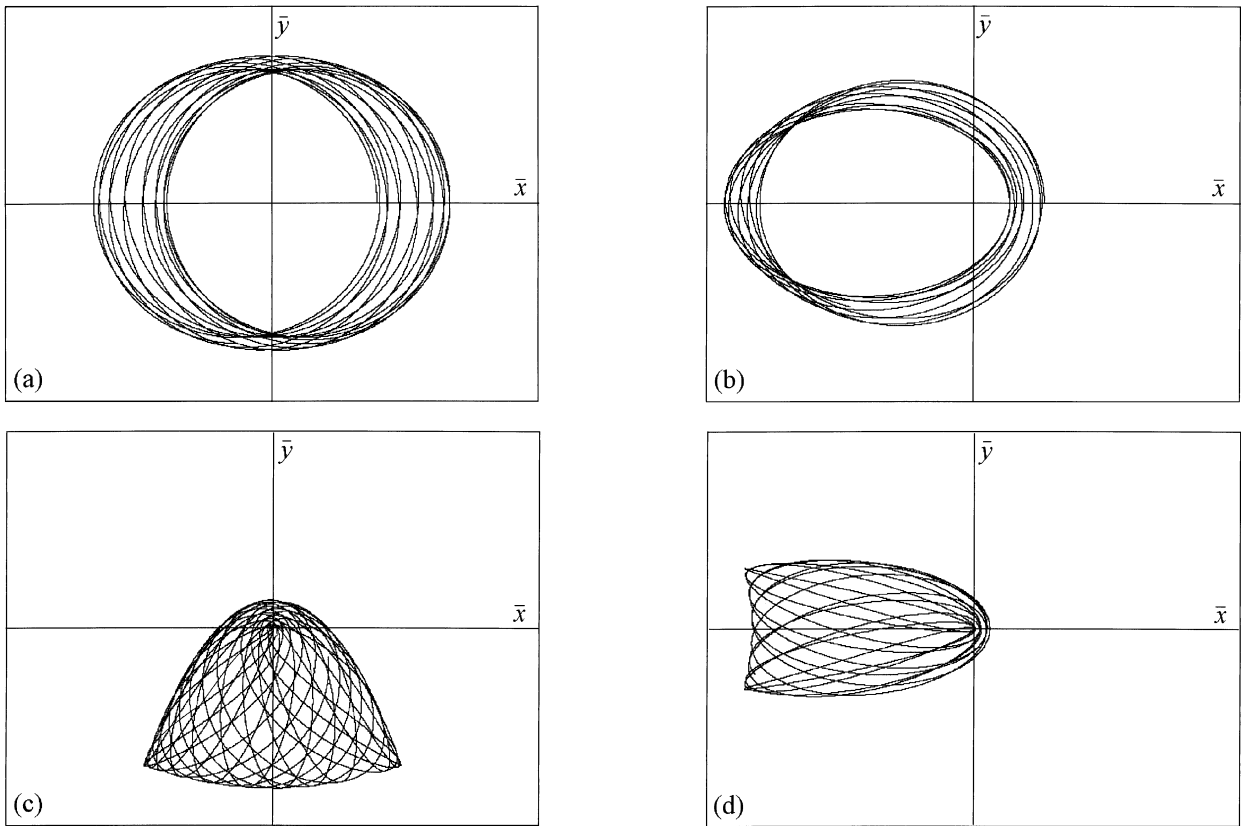


Figure 4. The shapes of the tube and lens orbits for $e_1 = 0.2$: (a) a circular tube for $M_b/M_g = 0.04$; (b) a long-axis elliptical tube for $M_b/M_g = 0.025$; (c) a short-axis lens orbit for $M_b/M_g = 0.04$; (d) a long-axis lens orbit for $M_b/M_g = 0.06$.

for greater values of M_b/M_g , because there is no natural evidence for the existence of such large mass fractions. As it can be seen in Figs 3(e) and (f), the inclined radial motions remain unstable. In fact, their stability implies the existence of ‘inclined lenses’, which are inconsistent with the assumed density distribution of the host galaxy.

To generate the orbits shown in Fig. 4, we choose an arbitrary initial point on a pre-selected phase-space curve of Fig. 3. Then, from equations (24) and (17) we determine the corresponding initial values of Q_1 , Q_2 and Q_3 and numerically integrate the averaged equations (22) over the specified phase-space trajectory. The temporal histories of g' and G' are then found by

$$g' = \frac{1}{2} \arctan \frac{Q_2}{Q_1},$$

$$G' = 2\Omega Q_3. \quad (33)$$

Furthermore, we know that L' is a constant and $\ell' = \Omega\tau + \ell'_0$ where ℓ'_0 is the initial value of ℓ' . Therefore, the temporal histories of ℓ , g , L and G are found by the mapping (14). Substitution of the results into (11) and then into (8) yields the orbit of the test particle in the \bar{x} - \bar{y} plane. The accuracy of orbits generated by this scheme is of $\mathcal{O}(\epsilon^2)$, which is enough for our investigation.

7 DISCUSSIONS AND CONCLUSIONS

The numerical study of stellar systems with central singularities shows a sensitive dependence of orbital evolution on the mass of

compact nuclear objects. Currently available observational data indicate that the mass fraction M_b/M_g is limited to values smaller than 0.03. Thus, greater values of M_b/M_g should be somehow ruled out. Our ‘finite’-mass model based on the density distribution (1) allowed us to investigate the sensitivity of orbital structure to the growth of M_b/M_g . The potential function associated with (1) has a polynomial form, which is generally non-integrable. Besides this, a central Newtonian cusp contributes a fractional term to the Hamiltonian function that seems to be inconsistent with the potentials of polynomial type. One can overcome this problem by expressing the dynamics in the well-known Delaunay variables. As the mean anomaly does not explicitly occur in the Hamiltonian function, the cost of higher order averaging (orders greater than 1) increases considerably. By using the Levi-Civita transformation, however, we are able to express our Hamiltonian only in polynomial functions that are appropriate for the application of Deprit’s (1969) normalization procedure up to any desired order.

7.1 Limitations of the model

High-resolution observations based on *Hubble Space Telescope* photometry of nearby galaxies have revealed that giant ellipticals have power-law surface density distributions near the centre. Therefore, our density function with a smooth core, defined by equation (1), does not seem to be realistic. We have chosen such a distribution for several reasons.

(1) In order to work with the mass fraction M_b/M_g , M_g should be

finite. Unfortunately, known cuspy models do not have such a property. Thus, we have to adopt a finite-mass model.

(2) Analytical methods can easily be carried out for models with finite cores. Moreover, the models with smooth cores have been extensively used in the construction of self-consistent equilibrium states (see Levine & Sparke 1998 and references therein).

(3) MQ use the following density distribution:

$$\rho(m^2) = \frac{\rho_0 m_0^2}{(1+m^2)(m_0^2+m^2)}, \quad 0 \leq m_0 \leq 1, \quad (34)$$

where m_0 and ρ_0 are the core radius and central density, respectively. This model resembles real elliptical galaxies and bulges. Sufficiently near the centre we have $m < m_0$. For such a circumstance, one can expand the right-hand side of (34) as a Taylor series and obtain

$$\rho(m^2) \approx \rho_0 \left[1 - \left(1 + \frac{1}{m_0^2} \right) m^2 \right]. \quad (35)$$

It can be readily verified that equation (35) yields a gravitational potential similar to (3).

Our study is credible within the sphere of influence of the BH ($h < 0$) where the equations of motion are integrable asymptotically. In the outer regions, however, the normalization procedure adopted here breaks down and the phase space is populated by stochastic orbits.

7.2 Evolving toward axisymmetry and possible self-consistent states

As the lenses originate from the radial motions, stars moving in such orbits pass very close to the centre. These stars may be shredded or supplied as fuel for the nucleus. Therefore, in the construction of self-consistent equilibrium states, the lenses must be treated cautiously.

Consider a strongly non-axisymmetric potential similar to our second example ($e_1 = 0.2$). Geometries like those shown in Fig. 3 appear sequentially. At first only the lenses are present for sufficiently small values of M_b/M_g . The lenses can supply the fuel needed for the growth of the BH. As the BH mass grows, the long-axis lenses are swept out and the long-axis elliptical tubes emerge. The mass of the BH can still increase, because of the presence of the short-axis lenses. As long as the elliptical tubes fill a portion of phase space, the model can maintain its non-axisymmetric structure in the central regions. Once the elliptical tubes disappear, the circular tubes occur and cause the orbital content to become rounder. This effectively cuts off the fuel supply of the nucleus and controls the growth of the BH mass. Hence, it would be logical to assume that the system never reaches a stage similar to that shown in Fig. 3f. In both circular and elliptical tubes, the orbital angular momentum, G , takes its minimum near the major axis where the model density is maximum. This is the sign of self-consistency, which can be checked by the method developed by Zhao et al. (1999). Nevertheless, our results show that there is a limited band for those values of M_b/M_g that support the existence of elliptical tubes, and, in consequence, the highly non-axisymmetric shapes of orbits. For moderate values of e_1 , the behaviour of the system is governed by a geometry similar to Fig. 2 that speeds up evolution toward axisymmetry.

The mechanism of evolution toward axisymmetry mentioned

here is different from that presented in MQ, because we are only confined to regular orbits within the BH sphere of influence. The overall shape of the galaxy cannot be determined by the regular families of orbits presented here. A treatment based on stochastic orbits, like that of MQ, would be helpful for this concern.

ACKNOWLEDGMENTS

The author thanks S. Sridhar for reading the first draft of the paper and for useful suggestions. The referee Giuseppe Pucacco provided illuminating comments to improve the presentation of the results. This work was supported by IASBS.

REFERENCES

- Boccaletti D., Pucacco G., 1996, *Theory of Orbits*, Springer, Berlin
 Chandrasekhar S., 1969, *Ellipsoidal Figures of Equilibrium*, Yale Univ. Press, New Haven
 Deprit A., 1969, *Celest. Mech.*, 1, 12
 Deprit A., 1991, *Celest. Mech.*, 51, 201
 Deprit A., Elipse A., 1991, *Celest. Mech.*, 51, 227
 de Zeeuw P. T., Merritt D., 1983, *ApJ*, 267, 571
 Goodman J., Binney J., 1984, *MNRAS*, 207, 511
 Jalali M. A., Sobouti Y., 1998, *Celest. Mech.*, 70, 255
 Kormendy J., Richstone D. O., 1995, *ARA&A*, 33, 581
 Levine S. E., Sparke L. S., 1998, *ApJ*, 503, 125
 Merritt D., Quinlan G. D., 1998, *ApJ*, 498, 625(MQ)
 Merritt D., Valluri M., 1996, *ApJ*, 471, 82
 Sridhar S., Touma J., 1997, *MNRAS*, 287, L1
 Sridhar S., Touma J., 1999, *MNRAS*, 303, 483 (ST)
 Zhao H. S., Carollo C. M., de Zeeuw P. T., 1999, *MNRAS*, 304, 457

APPENDIX A: CONSTANT COEFFICIENTS IN THE POTENTIAL U

One can readily verify from (2) that

$$a_{00} = \int_0^\infty \frac{du}{\sqrt{1+u}\sqrt{e_1^2+u}\sqrt{e_2^2+u}}, \quad (A1)$$

$$a_{11} = \int_0^\infty \frac{du}{(1+u)^{3/2}\sqrt{e_1^2+u}\sqrt{e_2^2+u}}, \quad (A2)$$

$$a_{22} = \int_0^\infty \frac{du}{(e_1^2+u)^{3/2}\sqrt{1+u}\sqrt{e_2^2+u}}, \quad (A3)$$

$$a_{33} = \int_0^\infty \frac{du}{(e_2^2+u)^{3/2}\sqrt{1+u}\sqrt{e_1^2+u}}, \quad (A4)$$

$$a_{12} = \int_0^\infty \frac{du}{(1+u)^{3/2}(e_1^2+u)^{3/2}\sqrt{e_2^2+u}}, \quad (A5)$$

$$a_{13} = \int_0^\infty \frac{du}{(1+u)^{3/2}(e_2^2+u)^{3/2}\sqrt{e_1^2+u}}, \quad (A6)$$

$$a_{23} = \int_0^\infty \frac{du}{(e_1^2+u)^{3/2}(e_2^2+u)^{3/2}\sqrt{1+u}}, \quad (A7)$$

$$b_{11} = \int_0^\infty \frac{du}{(1+u)^{5/2}\sqrt{e_1^2+u}\sqrt{e_2^2+u}}, \quad (A8)$$

$$b_{22} = \int_0^\infty \frac{du}{(e_1^2+u)^{5/2}\sqrt{1+u}\sqrt{e_2^2+u}}, \quad (A9)$$

$$b_{33} = \int_0^\infty \frac{du}{(e_2^2 + u)^{5/2} \sqrt{1+u} \sqrt{e_1^2 + u}}. \quad (\text{A10})$$

APPENDIX B: CONSTANT COEFFICIENTS IN THE NORMALIZED HAMILTONIAN

The constant coefficients c_i ($i = 1, \dots, 8$) are found to be

$$c_0 = \xi^3(\lambda^2 + \omega^2),$$

$$c_1 = 6\xi(\lambda^2 + \omega^2),$$

$$c_2 = 10\xi(\omega^2 - \lambda^2),$$

$$c_3 = -\xi^5 \left\{ \frac{1}{4}(3\alpha + 3\gamma + 2\beta) + \frac{1}{\Omega^2} \left[\frac{35}{6}(\omega^4 + \lambda^4) + \frac{73}{3}\omega^2\lambda^2 \right] \right\},$$

$$c_4 = -\xi^3 \left\{ 5(3\alpha + 3\gamma + 2\beta) + \frac{1}{3\Omega^2} [638(\omega^4 + \lambda^4) + 236\omega^2\lambda^2] \right\},$$

$$c_5 = -\xi \left\{ \frac{15}{2}(3\alpha + 3\gamma + 2\beta) + \frac{1}{3\Omega^2} [1229(\omega^4 + \lambda^4) - 802\omega^2\lambda^2] \right\},$$

$$c_6 = \xi \left[\frac{63}{2}(2\beta - \alpha - \gamma) - \frac{655}{3\Omega^2}(\omega^2 - \lambda^2)^2 \right],$$

$$c_7 = \xi^3 \left[21(\gamma - \alpha) - \frac{262}{\Omega^2}(\omega^4 - \lambda^4) \right],$$

$$c_8 = \xi \left[42(\gamma - \alpha) - \frac{524}{\Omega^2}(\omega^4 - \lambda^4) \right],$$

where $\xi = L'/\Omega$. From (16), (17) and (18) one can show that

$$C_0 = \Omega^2 \xi + c_0 + \frac{1}{2}c_3, \quad (\text{B1})$$

$$A_{10} = c_1 - c_2 + \frac{1}{2}c_4 - \frac{1}{2}c_7, \quad (\text{B2})$$

$$A_{12} = c_5 + c_6 - c_8, \quad (\text{B3})$$

$$A_{20} = c_1 + c_2 + \frac{1}{2}c_4 + \frac{1}{2}c_7, \quad (\text{B4})$$

$$A_{21} = c_5 + c_6 + c_8, \quad (\text{B5})$$

$$C = c_5 - 3c_6. \quad (\text{B6})$$

This paper has been typeset from a \TeX/L\AA\TeX file prepared by the author.